



# Assessment of RELAP5 matrix solvers for a two-phase natural circulation loop

Francisco A. Braz Filho <sup>a</sup>, Gaianê Sabundjian <sup>b</sup>, Guilherme B. Ribeiro <sup>a,\*</sup>, Alexandre D. Caldeira <sup>a</sup>

<sup>a</sup> Institute for Advanced Studies, Aerospace Science and Technology Department, São José dos Campos, Brazil

<sup>b</sup> Nuclear and Energy Research Institute, National Nuclear Energy Commission, São Paulo, Brazil



## ARTICLE INFO

### Article history:

Received 22 February 2017

Received in revised form 13 March 2017

Accepted 14 March 2017

Available online 27 March 2017

### Keywords:

Natural circulation

Transient

Solver

Two-phase

RELAP5

## ABSTRACT

The heat transfer mechanism of natural convection has been extensively studied as a passive heat removal system of new nuclear power plants. Considering this aspect, the main objective of this study is to present an assessment of RELAP5 linear-equation solver under a transient two-fluid model for a two-phase natural circulation loop (NCL). For this assessment, three different approaches of linear-equation solvers for the hydrodynamic model are presented: the sparse matrix solver based on the Lower-Upper (LU) decomposition, the Border-Profile Lower Upper (BPLU) solver and the iterative method named Generalized Minimal Residual Method (GMRES). For comparison purposes, an experimental natural circulation loop made of glass tubes and using water as working fluid is analyzed. The onset of nucleate boiling observed during the experiment was predicted by all RELAP5 solvers as well as the representation of flow oscillations along the loop. Furthermore, it was noticed that the choice of the solver algorithm has a strong influence on the prediction of the two-phase natural circulation phenomena, since different wavelengths and amplitudes of flow instabilities were obtained for each approach.

© 2017 Published by Elsevier Ltd.

## 1. Introduction

Passive systems such as Natural Circulation Loop (NCL) play an important role in the safety of nuclear power plants, mostly due to the fact that any power supply is unnecessary (Jaluria and Torrance, 1986). Advanced reactors have been designed using passive safety systems based on natural circulation (Braaten and Shyy, 1987). Furthermore, other aspects like simplification and economy explain why natural convection is the chosen heat removal mechanism at reactor cores, especially after the accident occurred at the Fukushima Daiichi power plant. Thus, the use of passive heat removal systems is one of technologies that is being considered for the “Generation IV” nuclear energy systems (Hittner, 2006; Vaghetto and Hassan, 2014).

Considering all the advantages aforementioned, water-cooled NCL has found application in different areas like cooling of electronic components, geothermal processes, natural gas processing plants and solar powered heaters. Thus, the need to study and assess the heat transfer and fluid flow characteristics of water natural convection phenomena under typical conditions found in nuclear applications is crucial. A detailed review of the state-of-

the-art of NCL, its applications and research trends was performed by Basu et al. (2014).

For this type of heat transfer transport, the density gradient provided by the difference of temperature results in buoyancy forces which drives the water along the loop. Water is heated at the lower part of the loop, bubbles are nucleated and after detachment they rise due to buoyancy forces. After that, the fluid is condensed at the heat sink, becomes denser at the higher part of the loop, and then moves downwards and completes the natural convection loop.

Several studies related to single phase and two-phase flow natural convection have been addressed in the last years. Vijayan (2002) performed a review of non-dimensional groups applied at NCL and then suggested a correlation based on geometric parameters and the Grashof number for the prediction of the steady state single-phase flow. In addition, it was observed that the stability behavior of the natural circulation loop depends also on the modified Stanton number. Misale et al. (2007) and Misale and Garibaldi (2012) studied experimentally the thermal-hydraulic performance of a natural circulation mini-loop using distilled water and a nanofluid with different concentrations of  $\text{Al}_2\text{O}_3$ . The mini-loop was placed onto a table and the influence of its inclination was investigated. Data results were compared with the Vijayan correlation, showing a satisfactory agreement.

\* Corresponding author.

E-mail address: [gbriveiro@ieav.cta.br](mailto:gbriveiro@ieav.cta.br) (G.B. Ribeiro).

## Nomenclature

ARL	auxiliary refrigerating leg
BPLU	border Profile Lower–Upper method
GMRES	generalized minimum residual method
LU	Lower–Upper method

NCL	natural circulation loop
STHX	spiral tube heat exchanger
TFM	two-fluid model

Sarkar and Basu (2016) conducted numerically a thermal-hydraulic comparison between super-critical carbon dioxide and subcritical water for NCL, applying identical conditions at the heat source and heat sink. It was observed that the heat transfer deterioration restricts the use of supercritical fluids at high temperatures. With the intention to evaluate the effect of mass flow rate due to heat flux changes and stability, Rabiee et al. (2016) constructed a NCL using atmospheric conditions. Additionally, numerical simulations of the loop were performed via RELAP5 in order to analyze the thermal hydraulic parameters on the stability of the operating conditions. As a manner to improve the NCL performance, Goudarzi and Talebi (2015) applied the entropy generation minimization method where the governing equations of the entropy generation were solved analytically. Several studies focusing on the modeling of the NCL characteristics via CFD technique appeared recently and, among these studies, the work of Pal et al. (2016), Tung et al. (2014) and Wang et al. (2013) can be highlighted.

Focusing on electromagnetic problems, Puzyrev et al. (2016) performed an assessment of direct solvers where the computational demands, parallel scalability and robustness were compared. Typical state-of-the-art finite-element and finite-difference problems were used for the tested solvers. In that study, the Watson Sparse Matrix Package was considered as a promising solver for high performance computation. As a manner to enhance the transient and 3D flow simulation for wind and marine turbines, Mycek et al. (2017) compared three iterative linear-equation solving algorithms: Jacobi, CG (Conjugate Gradient) and Bi-CGSTAB (Bi-Conjugate Gradient Stabilised). Numerical simulations have proved that Bi-CGSTAB is more efficient than the others.

Considering all the foreseen aspects, this study intends to contribute to this research field, providing a numerical assessment of different linear-equation solvers available at the RELAP5 code, under a typical natural convection application. Each solver technique provides different accuracy levels, when compared to the experimental data. Therefore, under tested conditions, the influence of the solver on the onset of nucleate boiling and on the prediction of two-phase flow instability is assessed.

## 2. Thermal-hydraulic model

The RELAP5 provides several mathematical modeling and, regarding the thermal-hydraulic model, it applies the finite-difference method in order to solve Partial Differential Equations (PDEs) related to the Two Fluid Model (TFM). With this modeling each phase (liquid and vapor) has its own set of three governing equations (i.e., mass, momentum and energy equations), while interfacial interactions are represented as source terms. Thus, the mass conservation for phase  $k$  under a one-dimensional transient flow is represented as

$$\frac{\partial}{\partial t}(\alpha_k \rho_k) + \frac{1}{A} \frac{\partial}{\partial x}(\alpha_k \rho_k u_k A) = M_k, \quad (1)$$

where  $\alpha$ ,  $\rho$  and  $u$  are the void fraction, density and velocity, respectively. Variable  $A$  denotes the channel flow area, whereas  $M$  is the

volumetric mass exchange rate. The momentum conservation equation is described as

$$\begin{aligned} \alpha_k \rho_k A \frac{\partial u_k}{\partial t} + \frac{1}{2} \alpha_k \rho_k A \frac{\partial u_k^2}{\partial x} \\ = -\alpha_k A \frac{\partial P}{\partial x} + \alpha_k \rho_k B_x A - (\alpha_k \rho_k A) Fw_k \cdot u_k + \Gamma_k A (u_{k,i} - u_k) \\ - (\alpha_k \rho_k A) Fi_k \cdot (u_k - u_r) - \alpha_k \alpha_r \rho_m A \left[ \frac{\partial (u_k - u_r)}{\partial t} + u_r \frac{\partial u_k}{\partial x} - u_k \frac{\partial u_r}{\partial x} \right], \end{aligned} \quad (2)$$

where  $P$  is the pressure and  $B_x$  is the body force. Coefficients  $Fw$  and  $Fi$  are included as a manner to represent the wall drag and interfacial drag forces. The term  $\rho_m$  denotes the two-phase mixture density and  $u_r$  is the phase  $r$  velocity. The energy conservation equation is represented as

$$\begin{aligned} \frac{\partial}{\partial t}(\alpha_k \rho_k U_k) + \frac{1}{A} \frac{\partial}{\partial x}(\alpha_k \rho_k U_k u_k A) \\ = -P \frac{\partial \alpha_k}{\partial t} - \frac{P}{A} \frac{\partial}{\partial x}(\alpha_k u_k A) + Qw_k + Qi_k + \Gamma_i h_k + \Gamma w h''_k + D_k. \end{aligned} \quad (3)$$

In Eq. (3) presented above,  $U$  is the specific internal energy and  $D$  is the energy dissipation function Heat transfer rates at the wall and at the interface are denoted by terms  $Qw$  and  $Qi$ , whereas vapor generation rates at wall and at the interface are defined as  $\Gamma_i$  and  $\Gamma_w$ , respectively. The term  $h$  is the specific enthalpy and  $h'$  is the specific enthalpy for the interfacial mass transfer.

Further details about RELAP5 governing equations can be found in Roth and Aydogan (2014) and in the Idaho National Laboratory (2012) code manual. Moreover, the RELAP5 modeling discretizes the differential equations of the TFM in finite-difference equations that are partially implicit in time. Details about the semi-implicit numerical treatment implemented at RELAP5 are also given in the at Idaho National Laboratory (2012). The TFM is widely defined as an ill-posed problem (Drew and Passman, 1998), since the system of PDEs is non-hyperbolic and non-conservative (Keyfitz, 2001). Consequently, numerical solutions of ill-posed two-fluid problems are usually involved with numerical instabilities, and diffusion. Thus, it is expected that the chosen linear-equation solver plays a strong influence on the final results.

## 3. Matrix solver schemes

As mentioned, the TFM results in algebraic equations grouped in a linear time-advancement matrix. Like most of scientific computing applications, large sparse matrix eigenvalue problems appear at the RELAP5 modeling. Hence, each transport PDE provides a system of linear equations which is typically characterized as

$$\mathbf{A} \cdot \mathbf{X} = \mathbf{B}, \quad (4)$$

where  $\mathbf{A}$  is the square sparse coefficient matrix,  $\mathbf{X}$  is the vector of unknowns and  $\mathbf{B}$  is the source term vector. The numerical solution for TFM at RELAP5 is based on direct methods originating from Gaussian elimination or iterative methods (Atkinson, 1989). All numerical techniques are available at RELAP5 and can be chosen

at the simulation input. The direct methodology is considered as the default solver and due to this reason, it is the most frequently used solver at RELAP5 simulations. However, this type of method holds a strong influence on the computational cost and accuracy of the flow solution, since a high level of matrix sparsity is found in NCL simulations and direct methods deal with the null elements of matrix  $\mathbf{A}$ .

In the RELAP5 code, the direct methodology is represented by the direct Lower-Upper (LU) decomposition method (Golub and Van Loan, 1989) and by the Border-Profile Lower Upper (BPLU) solver (Idaho National Laboratory, 2012). The LU decomposition algorithm breaks the sparse matrix  $\mathbf{A}$  into two matrices,  $\mathbf{L}$  and  $\mathbf{U}$ . Matrix  $\mathbf{L}$  is characterized by null coefficients at and above the main diagonal, whereas matrix  $\mathbf{U}$  is characterized by null coefficients below the main diagonal. Therefore, the unknown vector  $\mathbf{X}$  is obtained directly by two consecutive steps as shown in the following equations:

$$\mathbf{L} \cdot \mathbf{Y} = \mathbf{B}, \quad (5)$$

and

$$\mathbf{U} \cdot \mathbf{X} = \mathbf{Y}, \quad (6)$$

The BPLU solver provides also the direct LU scheme, minimizing computational operations with null coefficients via matrix  $\mathbf{A}$  pre-conditioning. Thus, the BPLU was created to solve systems of linear equations with high sparseness and, due to this reason, it is ideal for interconnecting systems such as pipelines and circulation loops. The BPLU pre-conditioning executes a number of coefficient permutations of matrix  $\mathbf{A}$  according to matrix reordering techniques such as the Cuthill and McKee (1969). In the end, matrix  $\mathbf{A}$  has a new structure that can be solved efficiently and faster than the straightforward LU decomposition scheme. This new structure is named as border-profile form, since most of non-zero coefficients are placed in a close band following the matrix main diagonal, whereas the remaining non-zeros coefficients are found in the last columns at the right side or in the last rows at bottom side of the matrix. Therefore, the non-zero coefficients form an arrow shaped matrix  $\mathbf{A}$ , pointing down and to the right.

A brief example (Mesina, 2011) of a coefficient reordering in order to achieve a border-profile structure can be illustrated by considering a simple reactor vessel re-nodalization shown in Fig. 1, where the core (1–3), core by-pass (4–6), downcomer (7–8), lower plenum (9) and upper plenum (10) are represented.

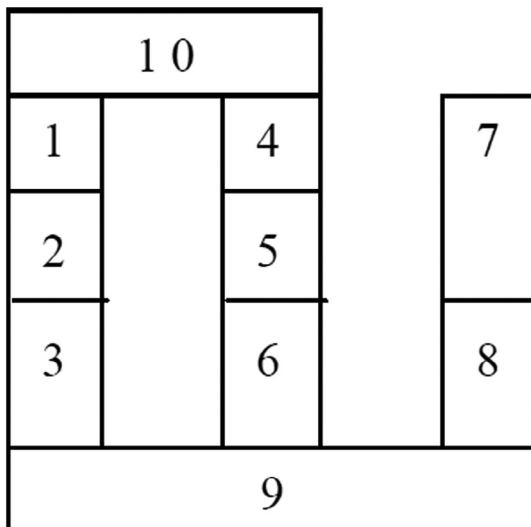


**Fig. 1.** Simplified reactor vessel nodalization for the BPLU matrix solver (Mesina, 2011).

The TFM combined with the BPLU solver results in the re-nodalization described above, generating an arrow-shaped  $10 \times 10$  matrix (with non-zero coefficients represented by  $a$ ), pointing down and to the right, as shown in Eq. (7). For the sake of simplicity, the null coefficients are not represented in the matrix.

$$A = \begin{bmatrix} a & a & & & & & & & & \\ a & a & a & & & & & & & \\ a & a & & a & & & & & & \\ & & a & a & & & & & & \\ & & a & a & a & & & & & \\ & & a & a & a & a & & & & \\ & & a & a & a & a & a & & & \\ & & a & a & a & a & a & a & & \\ & & a & a & a & a & a & a & a & \\ a & & a & & a & a & a & a & a & a \end{bmatrix} \begin{array}{l} | 1^{st} \text{node} \\ | 2^{nd} \text{node} \\ | 3^{rd} \text{node} \\ | 4^{th} \text{node} \\ | 5^{th} \text{node} \\ | 6^{th} \text{node} \\ | 7^{th} \text{node} \\ | 8^{th} \text{node} \\ | 9^{th} \text{node} \\ | 10^{th} \text{node} \end{array}. \quad (7)$$

With iterative characteristics, the RELAP5 code uses the Generalized Minimal Residual Method (GMRES) as a linear-equation solver. The GMRES algorithm was created especially for the numerical solution of large scale and non-symmetric linear systems. In this case, the Arnoldi iteration was implemented as the eigenvalue algorithm (Saad, 1992; Saad, 2003). In this study, the default convergence criteria were used at the NCL simulation run.

On the whole, these three aforementioned methods (i.e., LU, BPLU and GMRES) were used as solver algorithms in a typical NCL simulation. Due to the available settings, the LU solver was used at the RELAP5/MOD3 version, whereas the BPLU and GMRES solver were used at the RELAP5-3D. With the exception of the chosen solver, the same data input was applied for all simulations. As a manner of enhancing the assessment, numerical results were compared under the same initial conditions to an experimental test run.

#### 4. Experimental loop

The schematic figure of the experimental facility is shown in Fig. 2. Details about the setup and components have been described in the previous study of Sabundjian et al. (2011), so only essential information is described here. In order to allow the visualization of two-phase flow patterns, the loop has a rectangular cross-section made of glass. Two electrical heaters are installed inside the heated section, which consists in a 75 mm cylindrical glass tube. Both heaters dissipate the same amount of power input, providing 6536 W in the form of heat that is absorbed by the water.

The heat sink consists in a simple spiral copper tube heat exchanger (STHX), using water as working fluid for the auxiliary refrigeration leg (ARL). The heat sink section presents an internal diameter of 33 mm, with length of 610 mm. Furthermore, rotameters responsible for the measurement of the water flow rate were installed in the ARL. During the experiment, a mass flow rate of 0.023 kg/s (i.e., 84 kg/h) was kept constant with an inlet temperature of 20 °C at the STHX. The expansion tank acts as a pressurizer and is partially filled with water and opened to the ambient at the top end. At the bottom end, the expansion tank is attached to the loop, keeping the atmospheric pressure along the loop, despite any water specific volume change. Also, in order to prevent vapor admission to the expansion tank during experiments, the surge line is connected to the horizontal section of the cold leg.

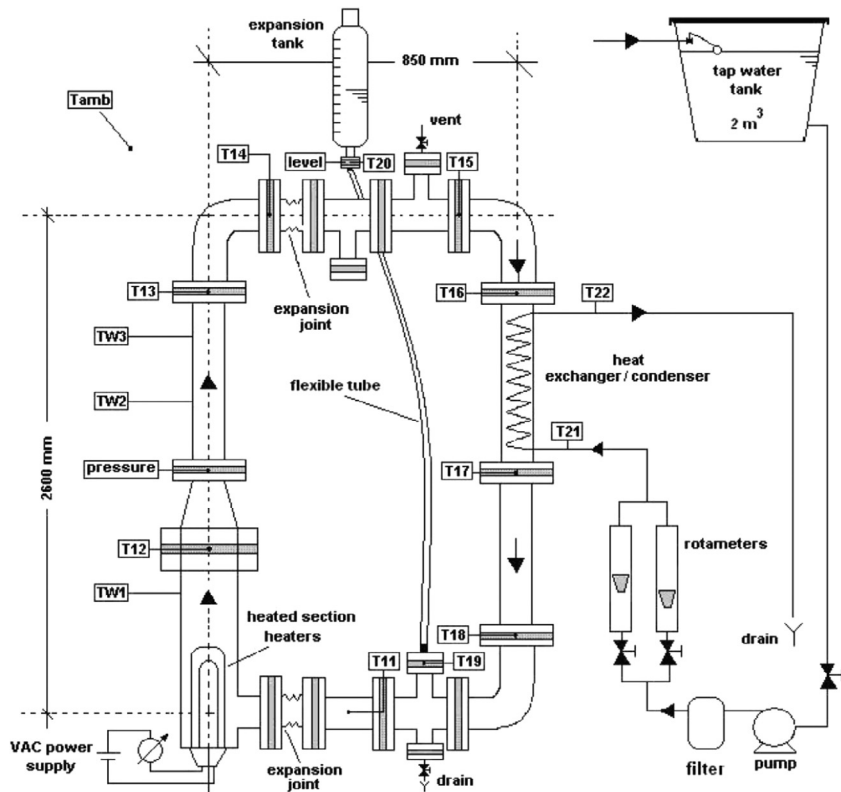


**Fig. 2.** Schematic figure of the natural circulation loop (Sabundjian et al., 2011).

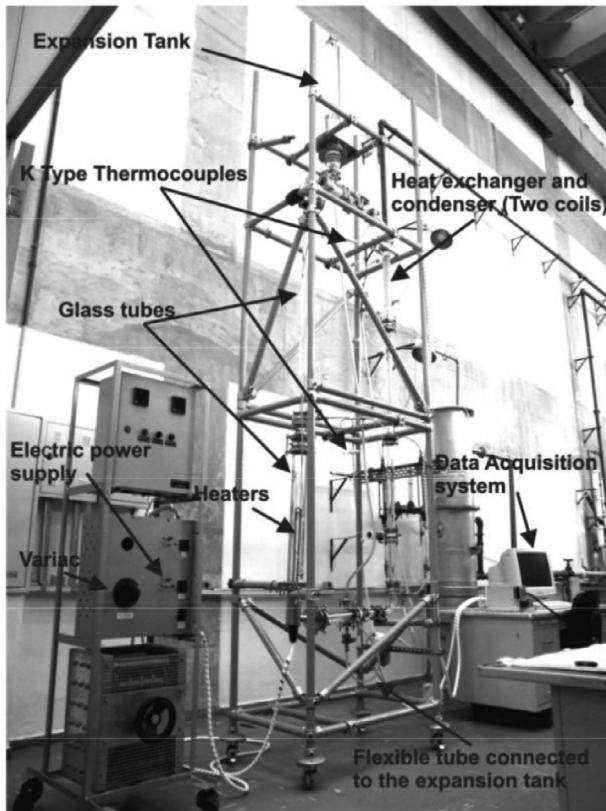


**Fig. 3.** Photograph of the natural circulation loop (Sabundjian et al., 2011).

Temperature measurements were performed using type-K thermocouples installed at fifteen locations: six measurements at the hot leg, four at the cold leg, two at the ARL inlet and outlet,

and three on the NCL external tube walls. All thermocouples have a measurement uncertainty of 1 °C. Additionally, a pressure meter is positioned at the heating section top. A sampling rate of 7 s was considered for the data acquisition process. The initial condition of 20 °C and 10<sup>5</sup> Pa (i.e., atmospheric pressure) was established for the test run. A photograph of the experimental facility can be seen in Fig. 3. In this study, the temperature measurements gathered from the heater outlet, STHX outlet and ARL outlet were used for solver assessments. The measurement are shown in Fig. 2 (positions T12, T17 and T22, respectively). The loop mass flow rate was not obtained experimentally, and only simulation data were used for the solver assessment.

## 5. Relap5 modelling

In order to simulate the thermal hydraulic behavior of the NCL, a proper one-dimensional nodalization was developed using pipe and branch components to represent the loop. As initial condition, all the volumes were filled with water except the volume representing the upper part of the expansion tank, which had also air inside. This model is able to predict the behavior for the single and two-phase experiments.

The saturation temperature is considered as the phase-change temperature, in the pressure of the circuit, disregarding the presence of non-condensable gases (i.e., 100 °C). RELAP5 nodalization is schematically presented in Fig. 4, and Table 1 shows the association of components between RELAP5 nodalization and the NCL. In Fig. 4, the size of the components is represented out of scale and do not represent the NCL dimensions.

The heating section is defined as pipe 100 with six subvolumes. The electric heater is represented as a heat structure with fixed heat flux attached to the first four subvolumes. In this modeling, the electric heater has no thermal losses and due to this reason the total dissipated heat is transferred to the water. The hot leg

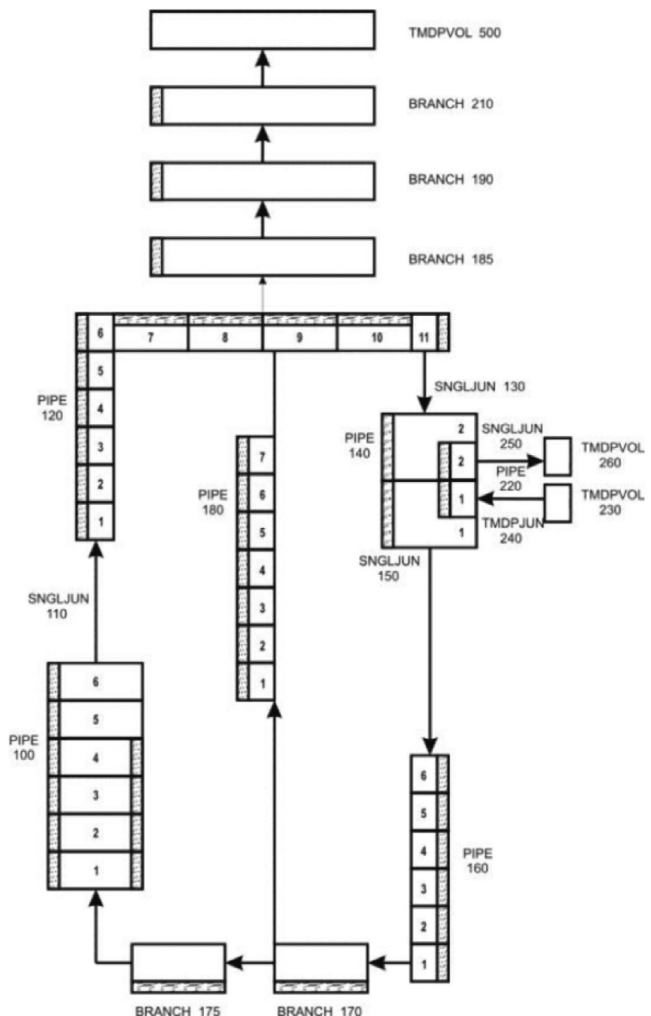


**Fig. 4.** Loop nodalization at RELAP5.

**Table 1**  
Nodalization of the natural circulation loop.

Component	Class number	Type
Heater	100	PIPE
Hot leg	120	PIPE
Heat sink outlet	140	PIPE
	150	SNGLJUN
Cold leg	160	PIPE
	170	BRANCH
	175	BRANCH
Surge line	180	PIPE
Expansion Tank	185	BRANCH
	190	BRANCH
	210	BRANCH
Auxiliary loop (inlet)	220	PIPE
	230	TMDPVOL
	240	TMDPJUN
Auxiliary loop (outlet)	250	SNGLJUN
	260	TMDPVOL
Containment	500	TMDPVOL

is represented by pipe 120 with eleven subvolumes and is connected to the heater pipe by the single-junction 110. The STHX was modeled as pipe 140 and has two single-junctions (130 and 150) which connect the STHX to the hot and cold leg. The cold leg and the surge line were modeled as pipes 160 and 180 and have six and seven subvolumes, respectively.

Moreover, the ARL was modeled using a simplified nodalization as represented by pipe 220 with two subvolumes, two time-dependent volumes (230 and 260), one time-dependent junction (240), and one single-junction (250). Constant flow rate and temperature of the ARL was imposed on the time-dependent junction 250, while the ambient temperature and atmospheric pressure were maintained on the discharge time-dependent volume 260.

The connection between the expansion tank and loop was enabled through the branch 170, while branches 185, 190 and 210 with the time-dependent volume 500 modeled the pressurizer. The atmospheric pressure is kept constant at the pressurizer via the time-dependent volume, whereas the three branches allow the water level monitoring.

With the exception of pipe 220, heat losses through the NCL wall are represented by a heat structure where a heat transfer coefficient of  $10 \text{ W/m}^2 \text{ }^\circ\text{C}$  and temperature of  $20 \text{ }^\circ\text{C}$  were combined with the conductive thermal resistance term related to the tube wall. For pipe 220, the heat structure is characterized by the wall thickness that separates the two fluid streams present in the STHX. Additionally, pressure drops due to change of flow direction in NCL elbows and due to flow contractions and expansions were introduced in the RELAP5 modeling via loss coefficients extracted from Idelchick and Fried (1986).

A fixed time step size of  $10^{-3}$  s was used for all simulation runs. Phase temperatures were calculated from phase internal energies via thermodynamic relationships, using the steam tables provided by Meyer et al. (1967). The volume temperature was characterized as the volume fraction-weighted average temperature of the liquid and vapor phase.

## 6. Results

**Fig. 5a-c** depict the temperature evolution of the heater outlet for the LU, BPLU and GMRES solvers, respectively. As can be seen in these figures, all solvers had similar results in the beginning of the transient regime, when the water temperature is increasing and natural single-phase convection is still the heat transfer mechanism. When compared with the experimental data, all simulation runs overestimated the heater outlet temperature during the single-phase regime. It is expected that improving the heat transfer coefficient estimation between NCL and ambient and also considering the heater thermal losses may enhance the agreement between the results.

When the saturation point is reached, the two-phase flow takes place and temperature oscillations occur due to bubble movement generated by buoyancy forces. The bubble motion provides a periodic flow pattern and the temperature and mass flow rate display a wave-like characteristic.

According to Fig. 5a–c, the onset of nucleate boiling started around 1250 s, for all numerical solvers and at the experimental facility. Thus, the time of the onset of nucleate boiling is well predicted by RELAP5 with any of the tested solvers used in this study. The difference between numerical results and experimental data within the two-phase region is expected since the numerical flow is considered one-dimensional and empirical correlations were applied for the computation of the heat transfer coefficient.

Regarding results depicted in Fig. 5a, the LU oscillations provided shorter wavelengths and lower amplitudes when compared to the experimental data. In comparison with other solvers, the LU scheme had the worst result when it comes to obtain the heater outlet temperature range. Additionally, according to Fig. 5b, it can be concluded that the BPLU solver promoted close wavelengths and lower amplitudes than the test run. When compared to the LU, the BPLU solver resulted in higher temperature amplitudes at the heater outlet. Furthermore, it can be also noticed that the

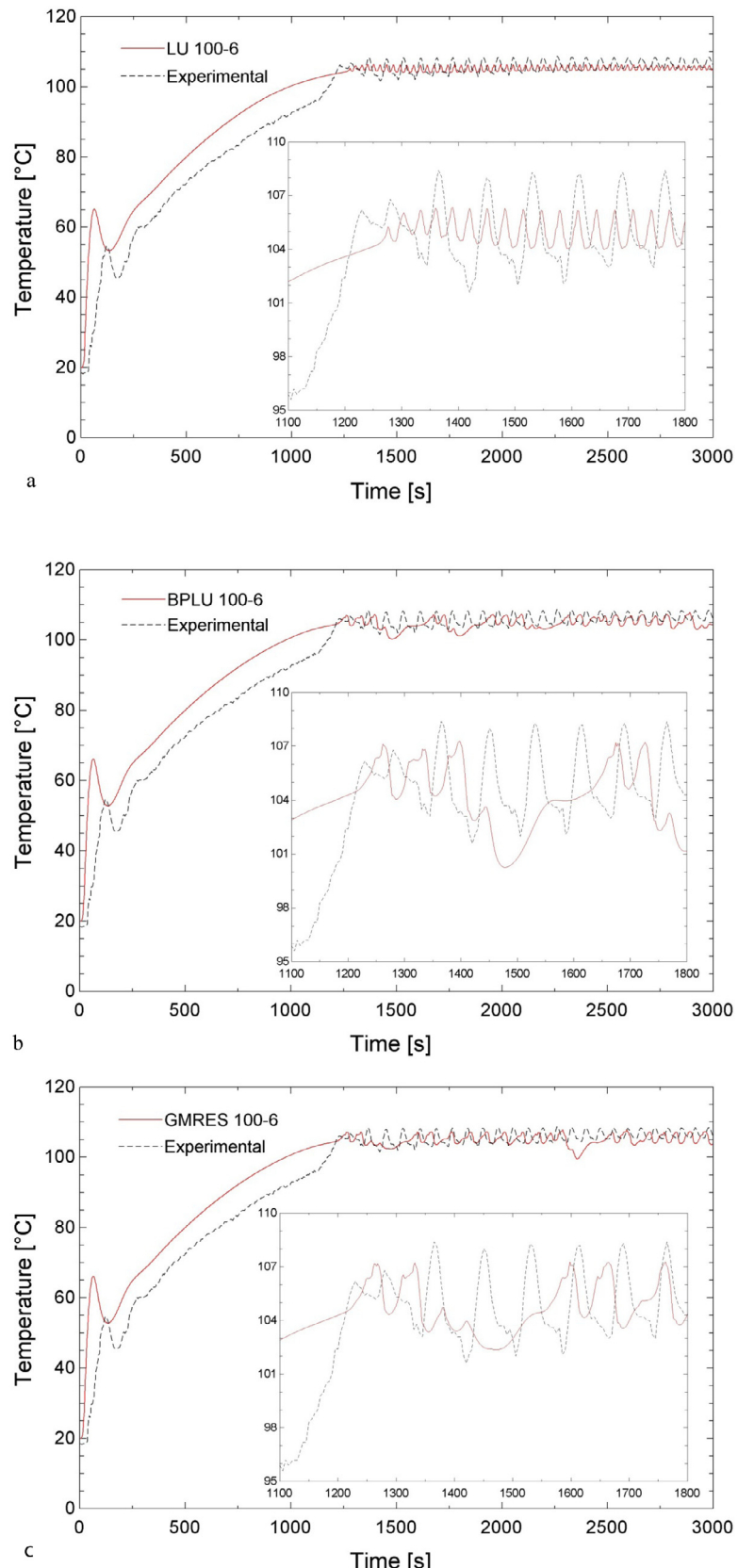


**Fig. 5.** a. Transient behavior of the heater outlet temperature with the LU solver. b. Transient behavior of the heater outlet temperature with the BPLU solver. c. Transient behavior of the heater outlet temperature with the GMRES solver.

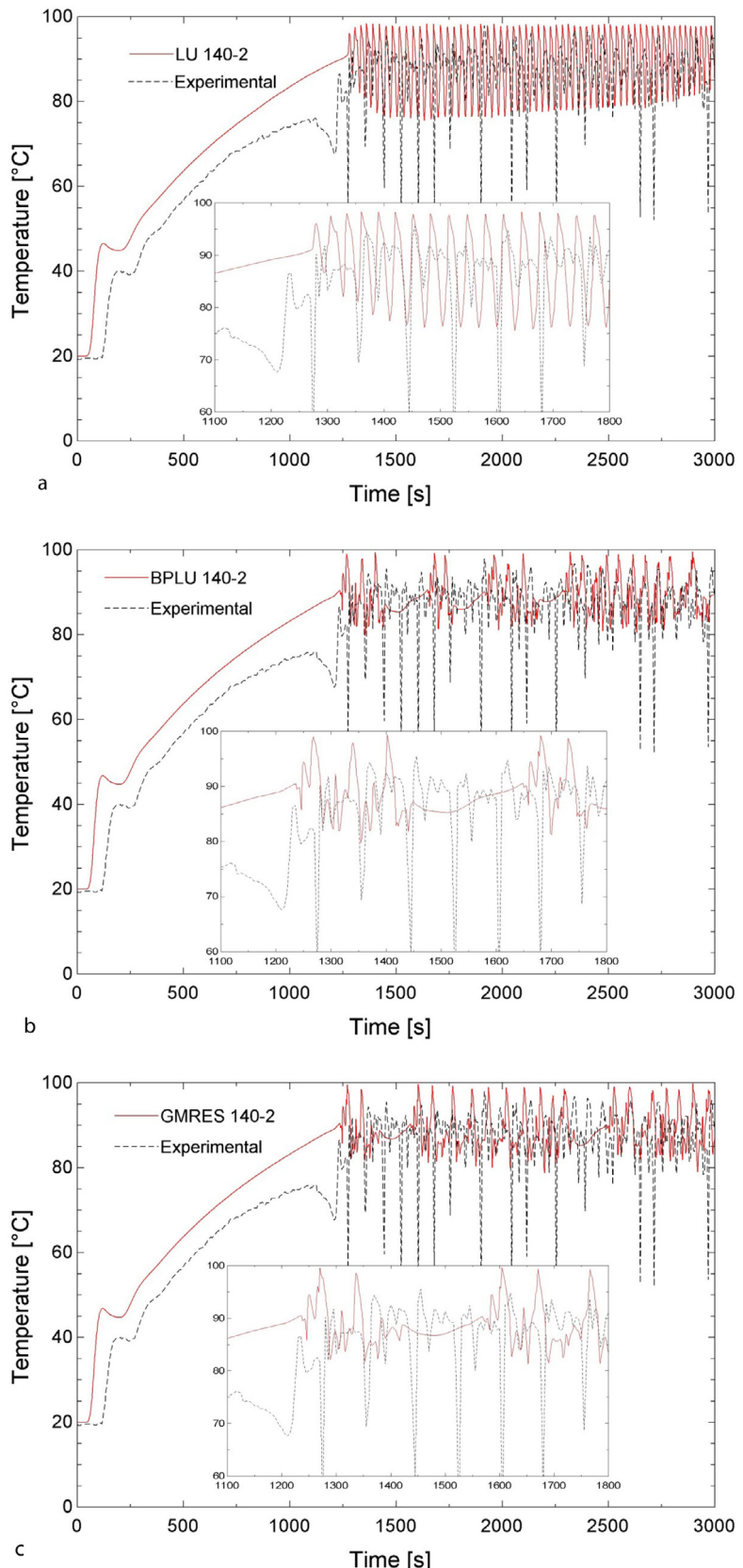


**Fig. 6.** a. Transient behavior of STHX outlet temperature with the LU solver. b. Transient behavior of STHX outlet temperature with the BPLU solver. c. Transient behavior of STHX outlet temperature with the GMRES solver.

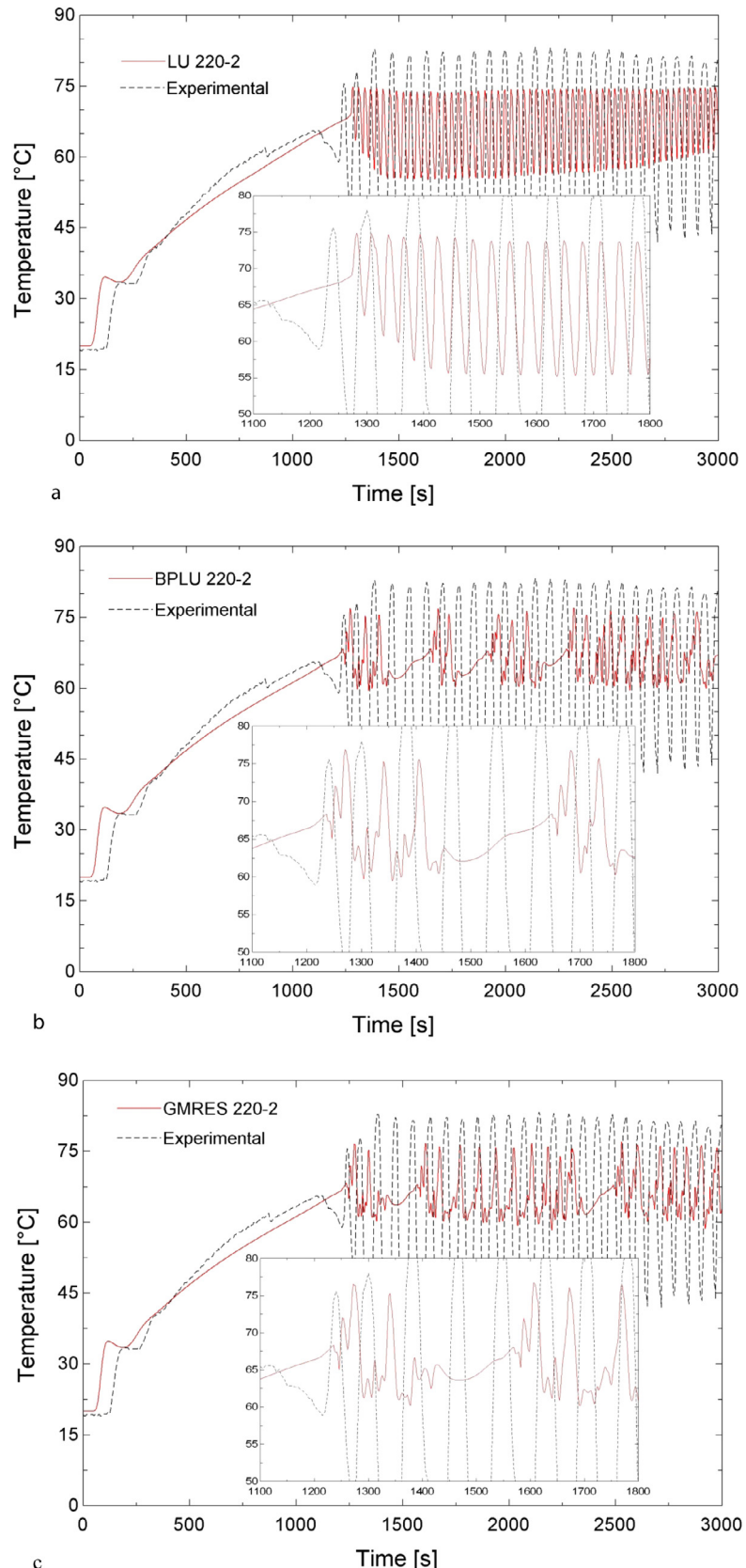


**Fig. 7.** a. Transient behavior of ARL outlet temperature with the LU solver. b. Transient behavior of ARL outlet temperature with the BPLU solver. c. Transient behavior of ARL outlet temperature with the GMRES solver.

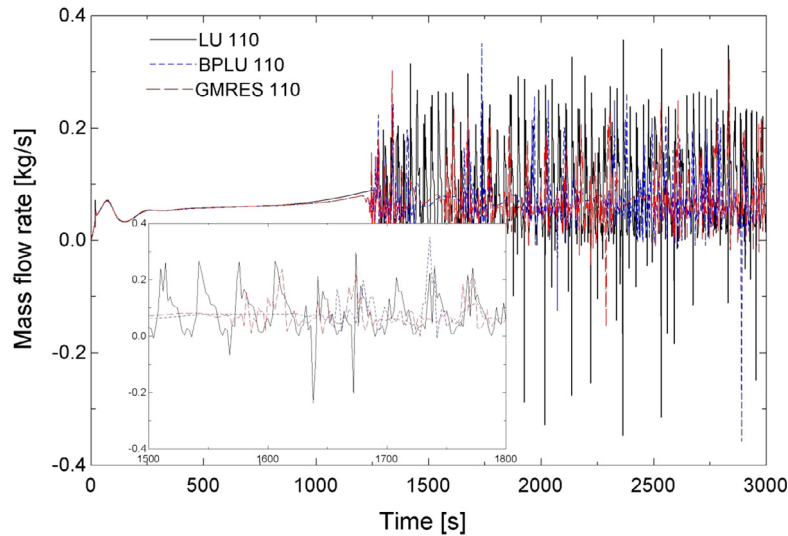


**Fig. 8.** Comparison of the mass flow rate at the NCL primary loop.

numerical modeling applied with the BPLU solver failed to show a clear periodic behavior in some short periods, as illustrated in Fig. 5b in the time frame from 1450 to 1650 s.

Similarly to the BPLU, the GMRES also failed to perform a periodic oscillation in some periods, as shown in the time frame from around 1350–1600 s in Fig. 5c. Nevertheless, the GMRES solving technique also performed a good agreement with the experimental data, when wavelengths are compared. Concerning the heater outlet temperature amplitude during the oscillating flow, BPLU and GMRES had similar results as well.

The transient behavior of the water temperature at the STHX outlet is presented in Fig. 6a–c for LU, BPLU and GMRES solvers, respectively. As expected, the STHX provided the water condensation and due to this reason temperatures below the saturation point were obtained during the flow time. As mentioned before, bubble nucleation and detachment caused mass flow rate instabilities that can be clearly seen at the STHX outlet. During early stages of the transient flow, during the NCL heating ramp-up, all solvers overestimate the temperature at the STHX outlet. Likewise the heater outlet, the onset of flow instabilities is well predicted by RELAP5, regardless of the numerical solver. Furthermore, comparing Fig. 6a–c, it can be inferred that the LU solver provided the shortest instability wavelength, while BPLU and GMRES presented close wavelengths. Regarding the temperature amplitude, it can be noticed that the LU scheme had higher amplitude than BPLU and GMRES. Again, Fig. 6b and c show in detail that BPLU and GMRES calculated similar flow instability amplitudes.

The water temperature at the ARL outlet for all the described solvers is displayed in Fig. 7a–c. As expected, these results also had flow instabilities due to the thermal contact with the NCL primary loop. Again, all solvers presented very similar results during the heating ramp-up. As evidenced by Fig. 7a–c, a good agreement was achieved among experimental data and solvers, before the oscillating flow. As can be seen by Fig. 7a–c, all numerical data provided lower temperature amplitudes than the experimental data. The numerical solution with the LU solver resulted in shorter wavelength. Considering the proposed solver methods, the BPLU and the GMRES solvers obtained a better agreement with the experimental data when wavelengths are compared. Likewise shown in Fig. 6b and c, BPLU and GMRES failed to represent flow oscillation during some periods of the simulation.

The RELAP5 result of the NCL mass flow rate can be seen in Fig. 8, applying all tested solving methods. As expected, the numer-

ical solution resulted in stable mass flow rate during single-phase flow and the two-phase flow instability is clearly characterized after 1250 s by irregular fluctuations of mass flow rate values. The onset of flow instability is predicted equally for all numerical methods, corresponding to the onset of nucleate boiling. In conformity with other results, the LU method had the shortest instability wavelength, followed by BPLU. Again, as evidenced by Fig. 8, BPLU and GMRES presented the longer oscillation wavelengths than LU. Regarding the flow oscillation amplitude, all solvers provided similar mass flow rate range.

## 7. Conclusions

It was seen that the study of natural convection as a heat removal mechanism can have a strong potential on the safety of nuclear power plants. Thus, a loop with natural circulation was simulated using different linear-equation solvers (LU, BPLU and GMRES). All of them apply the semi-implicit method for the time advancement of the TFM. For comparison purposes, experimental data provided by Sabundjian et al. (2011) were used along with the RELAP5 simulations.

Regardless the solving method, simulations showed that during the single-phase flow RELAP5 tended to over-predict the heater outlet and the STHX outlet temperature. A better estimation of the NCL thermal losses may enhance the prediction of the single-phase regime. Furthermore, RELAP5 was able to predict the onset of nucleate boiling and the onset of flow oscillations in the NCL. With regard to flow instabilities, the LU solver had the shortest wavelength, whereas the BPLU and GMRES solvers provided longer and similar wavelengths. When compared to the test run, solvers BPLU and GMRES provided a better agreement than the LU solver.

Regarding the flow amplitudes, all numerical solvers resulted in lower instability amplitudes than experimental data. Difference of instability amplitudes among the tested solvers was not evidenced.

## Acknowledgements

The authors would like to thank the Brazilian Air Force and the Chemical Engineering Department of University of São Paulo. Comments and suggestions of Roberto D. Garcia are highly appreciated.

## References

- Atkinson, K.A., 1989. An Introduction to Numerical Analysis. John Wiley & Sons, New York, ISBN 978-0-471-50023-0.
- Basu, D.N., Bhattacharyya, S., Das, P.K., 2014. A review of modern advances in analyses and applications of single-phase natural circulation loop in nuclear thermal hydraulics. *Nucl. Eng. Des.* 280, 326–348.
- Braaten, M.E., Shyy, W., 1987. Study of pressure correction methods with multigrid for viscous flow calculation in nonorthogonal curvilinear coordinates. *Numer. Heat Transfer* 11, 417–442.
- Cuthill, E., McKee, J., 1969. Reducing the bandwidth of sparse symmetric matrices. In: Proc. 24th National Conference of Association of Computing Machinery. pp. 157–172.
- Drew, D.A., Passman, S.L., 1998. Theory of Multicomponent Fluids, Applied Mathematical Sciences 135. Springer Verlag, New York, Berlin, Heidelberg.
- Golub, G.H., Van Loan, C.F., 1989. Matrix Computations. The Johns Hopkins University Press.
- Goudarzi, N., Talebi, S., 2015. Improving performance of two-phase natural circulation loops by reducing of entropy generation. *Energy* 93, 882–899.
- Hittner, D., 2006. RAPHAEL, a European project for the development of HTR/VHTR technology for industrial process heat supply and cogeneration. In: Proceedings of HTR 2006, 3rd International Topical Meeting on High Temperature Reactor Technology, October 1–4, Johannesburg, South Africa.
- Idaho National Laboratory, 2012. RELAP5-3D Code Manual Volume I: Code Structure, System Models and Solution Methods. Idaho National Engineering and Environmental Laboratory, Idaho Falls. INEEL-EXT-98-00834.
- Idelchick, I.E., Fried, E., 1986. Handbook of Hydraulic Resistance. Hemisphere Publishing, New York, NY.
- Jaluria, Y., Torrance, K.E., 1986. Computational Heat Transfer. Hemisphere, Washington, D.C.
- Keyfitz, B.L., 2001. Mathematical properties of nonhyperbolic models for incompressible two-phase flow. Proceedings of the International Conference of Mathematics of Fuzziness – ICMF.
- Mesina, G., 2011. BPPLU Completion and Verification Report. Idaho National Engineering and Environmental Laboratory, Idaho Falls. INEEL-EXT-11-23095.
- Meyer, C.A., McClintock, R.G., Silvestri, G.J., Spencer Jr., R.C., 1967. 1967 ASME Steam Tables – Thermodynamic and Transport Properties of Steam. The American Society of Mechanical Engineers, New York.
- Misale, M., Garibaldi, P., 2012. Experiments with Al<sub>2</sub>O<sub>3</sub> nanofluid in a single-phase natural circulation mini-loop: preliminary results. *Appl. Therm. Eng.* 40, 64–70.
- Misale, M., Garibaldi, P., Passos, J.C., Ghisi de Bitencourt, G., 2007. Experiments in a single-phase natural circulation mini-loop. *Exp. Therm. Fluid Sci.* 31, 1111–1120.
- Mycek, P., Pinon, G., Lothodé, C., Dezotti, A., Carlier, C., 2017. Iterative solver approach for turbine interactions: application to wind or marine current turbine farms. *Appl. Math. Model.* 41, 331–349.
- Pal, E., Kumar, M., Nayak, A.K., Joshi, J.B., 2016. Experimental and CFD simulations of fluid flow and temperature distribution in a natural circulation driven Passive Moderator Cooling System of an advanced nuclear reactor. *Chem. Eng. Sci.* 155, 45–64.
- Puzyrev, V., Koric, S., Wilkin, S., 2016. Evaluation of parallel direct sparse linear solvers in electromagnetic geophysical problems. *Comput. Geosci.* 89, 79–87.
- Rabiee, A., Mirzaee, M.M., Nematollahi, M.R., Atf, A., 2016. Experimental and numerical investigation of natural circulation stability of the SHUNCL thermal-hydraulic loop. *Prog. Nucl. Energy* 93, 386–396.
- Roth, G.A., Aydogan, F., 2014. Theory and implementation of nuclear safety codes – Part I: conservation equations, flow regimes, numerics and significant assumptions. *Prog. Nucl. Energy* 76, 160–182.
- Saad, Y., 1992. Numerical Methods for Large Eigenvalue Problems. Manchester University Press. ISBN 0-7190-3386-1.
- Saad, Y., 2003. Iterative Methods for Sparse Linear Systems. Society for Industrial and Applied Mathematics, ISBN 0-89871-534-2.
- Sabundjian, G., Andrade, D.A., Umbehaun, P.E., Torres, W.M., Macedo, L.A., Conti, T. N., Mesquita, R.N., Angelo, G., 2011. Comparison between experimental data and numerical modeling for the natural circulation phenomenon. *J. Braz. Soc. Mech. Sci. Eng.* 33, 227–232.
- Sarkar, M.K.S., Basu, D.N., 2016. Numerical comparison of thermohydraulic aspects of supercritical CO<sub>2</sub> and subcritical water based natural circulation loop. *Nucl. Eng. Technol.* <http://dx.doi.org/10.1016/j.net.2016.09.007>.
- Tung, Y.H., Johnson, R.W., Ferng, Y.M., Chieng, C.C., 2014. Modeling strategies to compute natural circulation using CFD in a VHTR after a LOFA. *Nucl. Eng. Des.* 275, 80–90.
- Vaghetto, R., Hassan, Y.A., 2014. Modeling the thermal-hydraulic behavior of the reactor cavity cooling system using RELAP5-3D. *Ann. Nucl. Energy* 73, 75–83.
- Vijayan, P.K., 2002. Experimental observations on the general trends of the steady state and stability behaviour of single-phase natural circulation loops. *Nucl. Eng. Des.* 215, 139–152.
- Wang, J.Y., Chuang, T.J., Ferng, Y.M., 2013. CFD investigation flow and heat transfer characteristics in a natural circulation loop. *Ann. Nucl. Energy* 58, 65–71.